Article

Photocatalytic Removal of Antibiotics from Wastewater Using the CeO$_2$/ZnO Heterojunction

Nicolae Apostolescu, Ramona Elena Tataru Farmus, Maria Harja * , **Mihaela Aurelia Vizitiu, Corina Cernatescu, Claudia Cobzaru and Gabriela Antoaneta Apostolescu ***

Department of Chemical Engineering, "Cristofor Simionescu" Faculty of Chemical Engineering and Environmental Protection, "Gheorghe Asachi" Technical University of Iasi, 73, Prof.dr.doc. Dimitrie Mangeron Avenue, 700050 Iasi, Romania

* Correspondence: mharja@tuiasi.ro (M.H.); ganto@ch.tuiasi.ro (G.A.A.); Tel.: +407-4790-9645 (M.H.); +407-542-4231 (G.A.A.)

Abstract: CeO$_2$/ZnO-based photocatalytic materials were synthesized by the sol-gel method in order to establish heterojunctions that increase the degradation efficiency of some types of antibiotics by preventing the recombination of electron–hole pairs. The synthesized materials were analysed by XRD, SEM, EDAX, FTIR, and UV-Vis. After several tests, the optimal concentration of the catalyst was determined to be 0.05 g·L^{-1} and 0.025 g·L^{-1} for chlortetracycline and 0.05 g·L^{-1} for ceftriaxone. CeO$_2$/ZnO assemblies showed much better degradation efficiency compared to ZnO or CeO$_2$ tested individually. Sample S3 shows good photocatalytic properties for the elimination of ceftriaxone and tetracycline both from single solutions and from the binary solution. This work provides a different perspective to identify other powerful and inexpensive photocatalysts for wastewater treatment.

Keywords: photocatalyst; CeO$_2$/ZnO heterojunction; chlortetracycline; ceftriaxone

1. Introduction

In our constantly and rapidly evolving world, finding solutions to protect the environment has been a priority lately. Among the substances that improve our life, but also make it more difficult, antibiotics are indispensable products due to the positive health benefits, though they have negative effects on natural ecosystems. Antibiotics are necessary medicines; many of them are on the WHO list of essential medicines, and their consumption is continuously increasing [1,2]. Unfortunately, some of these substances are excreted from the body unmetabolized in percentages that vary depending on the compound (up to 80% for tetracycline [3]), and their accumulation in wastewater and soil causes complications [4–8]. The presence of antibiotics in wastewater and also in drinking water has been detected in small amounts, but this is quite alarming for environmental safety [2,9]. The use of antibiotics in excess also leads to the appearance of antibiotic-resistant microorganisms [5,6,10,11]. Antibiotic resistance is a current problem leading to a decrease in the effectiveness of these classes of drugs. Tetracycline and ceftriaxone are widely used to treat various bacterial infections and have been detected in wastewater at varying concentrations. They are stable over time in the complex wastewater mixtures and are difficult to remove using classic water treatment methods; they can adversely affect the wastewater treatment processes (for example the ammonia removal process or chemical oxygen demand removal). There are several ways to remove antibiotics and other contaminants from wastewater, such as adsorption, sonochemical processes, ozonation, membrane technology, aerobic or anaerobic treatment, phytoremediation, biogeochemical methods such as wetlands, chemical disinfection methods such as chlorination, electrochemical oxidation processes, osmosis and electro-osmosis, electro-flocculation, ionizing radiation, and hybrid technologies [8,10,12–24]. However, it seems that the most effective methods of reducing the level of antibiotics in water are the methods that involve photocatalysis

and advanced oxidation processes. Photocatalytic methods are preferable to others because they are financially inexpensive and effective at low antibiotic concentrations, and the photocatalytic materials used are stable and environmentally benign [25–31]. Over time, several semiconducting materials have been tested for photocatalytic activity, but good results have been obtained showing oxides, sulphides, and their composites. Oxide materials were chosen because they are stable and inert, and the combination of two oxides leads to improved semiconductor properties. Although the most studied photocatalytic material is TiO_2, the results obtained with other materials have shown promising results. Photocatalytic systems based on oxides from blocks d and f (with semiconductor properties) have given good results in eliminating or reducing some polluting compounds from wastewater. Semiconductor materials are particularly attractive for environmental remediation applications. If semiconductors are exposed to electromagnetic radiation with an energy intensity greater than or close to the value of the band gap (E_g), electron–hole pairs are generated (valence band–conduction band); as a consequence (e^-–h^+) pairs are able to initiate redox reactions. According to studies in the literature, a photocatalyst's activity can be increased by doping, which is the addition of a substance that modifies the band gap value slightly in regions where incident radiation (ultraviolet or visible) can be used efficiently, by forming heterostructures, or by including reaction accelerators in the system that have the purpose of producing more free radicals or preventing their recombination [31–33]. The photocatalytic activity is closely related to the physicochemical properties but also to the morphology and texture of the materials studied, so the synthesis techniques are often of great importance. In this study, we followed the efficiency of some zinc oxide and cerium dioxide heterostructured materials synthesized in our laboratory towards the photocatalytic degradation of a classical antibiotic (chlortetracycline) and a third-generation cephalosporin-type antibiotic—ceftriaxone. Cerium has exciting catalytic characteristics because 4d and 5p electrons sufficiently defend the 4f orbitals. Ceria or Cerium(IV) oxide is a versatile, inert, and physically and chemically stable material with multiple and diverse applications. Due to its hardness (Mohs scale 7), it was initially used as an abrasive material, but today it is used (alone or in binary or complex mixtures) in the field of heterogeneous catalysis (oxidation of hydrocarbons) or in the field of sensors, energy, and fuels such as solid oxide fuel cells, but also in water-splitting processes or photocatalysis [33–35]. CeO_2 applications in the dermato-cosmetics industry and in the biomedical field (antibacterial effect) should also be mentioned here [36–38]. It is also possible to combine two or more properties, such as the infrared filtering properties with the photocatalytic ones, to optimize practical applications. Zinc oxide also has physical and chemical properties that ensure numerous practical uses, since it is introduced into the composition of many products to improve their properties (e.g., UV or antimicrobial protection); ZnO (alone or together with other oxides) is used in environmental applications, in medical applications, or as a sensor [32,39–41]. Using ZnO or CeO_2 separately leads to fast recombination processes that decrease the photocatalytic efficiency. The reduction in recombination rate can occur through the combination of two or more oxides as new energy bands are formed. Zinc oxide and cerium dioxide work well together and, in most cases, have a synergistic effect when they are associated in practical applications. [34,40,41].

As we know, there are several available studies on CeO_2/ZnO applications, as heterostructures as well as individually [20,24,32,38]. However, here, PVA, Poly(vinyl alcohol) was used as a dispersant for heterostructure management, and the obtained material showed good results for the photocatalytic degradation of two antibiotics, separately and in admixture, for low doses of UV radiation and for a small amount of catalyst. The results of this study can serve as a starting point for further research on CeO_2/ZnO materials.
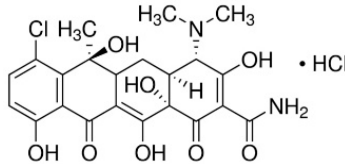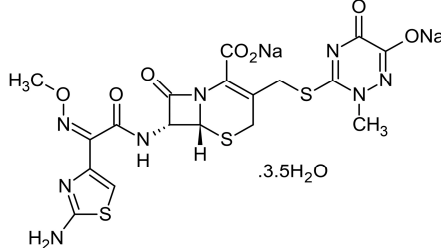
2. Materials and Methods

2.1. Reagents and Preparation

Photocatalytic materials were obtained by hydrothermal synthesis [42,43] starting from $Zn(CH_3COO)_2 \cdot 2H_2O$ and $Ce(NO_3)_3 \cdot 6H_2O$ (Sigma-Aldrich) as precursors and NH_4OH (25%

from Chemical Company, Romania) and PVA (average Mw 89,000–98,000, 99%, Aldrich) as anti-agglomeration agents. The precursors were mixed with ammonia solution in different molar ratios (S2- 2ZnO:CeO$_2$; S3- ZnO:2CeO$_2$), the mixture was kept at 120 °C for 8 h in a Teflon autoclave, and then the precipitates obtained were separated by centrifugation and washed with bidistilled water until the total elimination of NH$_4$OH, NH$_4$NO$_3$, and CH$_3$COOH. The precipitates thus obtained (cerium and zinc hydroxide) were immersed in a 0.001 mol·L^{-1} PVA solution for 30 min, filtered, and then calcined at 400 °C (at a heating rate of 5 grd·min^{-1}). Polyvinyl alcohol has the task of avoiding the agglomeration of particles and is eliminated by calcination. The samples obtained were named S1: ZnO, S2: 2ZnO-CeO$_2$, S3: ZnO-2CeO$_2$, and S4: CeO$_2$.

The antibiotics tested were chlortetracycline and ceftriaxone (Sigma Aldrich), presented in Table 1.

Table 1. Chemical structure and some characteristics of antibiotics.

Chemical Composition and Structure	Properties
CT—Chlortetracycline hydrochloride $C_{22}H_{23}ClN_2O_8 \cdot HCl$	The first antibiotic discovered and used; 515.34 g·mol^{-1} Solubility: 0.5–0.6 mg·mL^{-1} (20 °C) Biological half-life: 5.6–9 h Excretion mode: 60% renal, less than 10% biliary [44] Toxicology: 2.31 mg·kg^{-1} (LD50, mouse, oral) [45]
CFTX—Ceftriaxone $C_{18}H_{16}N_8Na_2O_7S_3 \cdot 3.5H_2O$	A third-generation antibiotic of the cephalosporin family; 661.60 g·mol^{-1} Melting point: 155 °C Solubility: 0.105 g·L^{-1} Biological half-life: 5.8–8.7 h Excretion mode: 33–67% renal, 35–45% biliary [46]

2.2. Sample Characterization

The synthesized samples were characterized by X-ray diffraction (Rigaku, Tokyo, Japan) and CuKα radiation (2θ angle, range from 10 to 80; step 0.02°/s); the possible functional groups remaining on the surface of the photocatalyst were identified by FTIR (Perkin Elmer Spectrum 100, PerkinElmer Inc., Shelton, CT, USA), resolution 2 cm^{-1} using 32 scans in the range 4000–400 cm^{-1}; all samples were prepared as KBr pellets (ratio 5/95 wt.%). The morphology of the prepared samples was observed with a Quanta 200 scanning electron microscope equipped with an energy-dispersive X-ray spectroscopy analyzer (Bruker Optics Inc, Billerica, MA, USA). The UV-Vis absorption spectra of the solid samples were obtained with a Jasco V-550 device (Jasco International CO, Kyoto, Japan) equipped with an integrating sphere. Monitoring of the photocatalytic degradation of antibiotics was performed also with a Jasco V-550 device (Kyoto, Japan).

2.3. Photodegradation Experiments

The magnetically stirred aqueous suspensions were UV-irradiated in a flat cylinder reactor (total volume: 100 cm^3) exposed to air. The radiant flux entering the reactor was about 0.21 mW·cm^{-2} (Hamamatsu C9536-01 m with H9958 detector for 310–380 nm), calculated from the distance between the samples and the light source produced by a UV-B lamp with Hg (18 W) (OSRAM, Munich, Germany). The volume of the solution was 75 cm^3, and the catalyst dose was 0.05 g·L^{-1}. Aqueous solutions were prepared using deionized

bidistilled water (Milli-Q, Millipore, Darmstadt, Germany). The degradation operations were carried out at room temperature at natural pH. The aerated suspension was first stirred in the dark for 40 min, which was sufficient to achieve equilibrated adsorption. The initial concentration was 0.025 mg·mL^{-1} chlortetracycline and ceftriaxone 0.05 mg·mL^{-1}.

The tests were performed without changing the pH of the native antibiotic solution. Samples were taken at fixed timed intervals and centrifuged to remove the solid, then the absorbance of the supernatant was read three times, noting the mean value. The level of antibiotic degradation was quantified using the correlation Equation (1):

$$R(\%) = \frac{(A_0 - A_i)}{A_0} \cdot 100 \tag{1}$$

where R(%) is the antibiotic degradation yield, A_0 and A_i are the initial and t_i time antibiotic absorbance values at the same time values.

3. Results and Discussion

3.1. Characterization of the Photocatalysts

The X-ray diffraction spectra of ZnO and CeO$_2$ and those of the as-synthesized composites are shown in Figure 1. They present several peaks that could be indexed in accordance with the diffraction spectrum of ZnO (JCPDS card no. 36-1451) and CeO$_2$ (JCPDS card no. 34-0394). For S1 (ZnO), the peaks were positioned at the 2θ angles: 31.83, 34.51, 36.32, 47.61, 55.64, 62.94, 68.03, and 69.16 can be indexed as (100), (002), (101), (102), (102), (103), (112), and (210), indicating a hexagonal wurtzite phase of ZnO; for S4 (CeO$_2$), the peaks were positioned at the 2 angle: 28.55, 56.44, 59.22, 69.37, 76.79, 79.11, and 88.48, which can also be indexed as (111), (311), (222), (400), (311), (420), and (422). The CeO$_2$ (111) peak is associated with the cubic structure. Samples S2 and S3 show the peaks corresponding to the polycrystalline structures of pure oxides, indicating the formation of composite materials with no other impurities [47–50].
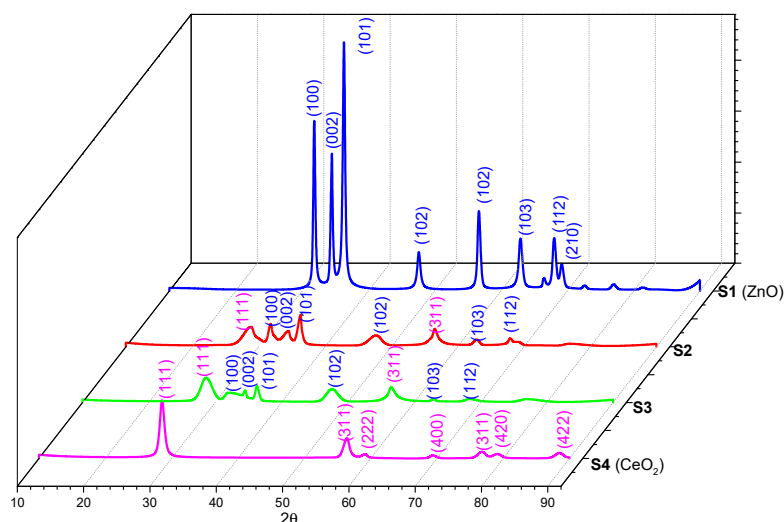
Figure 1. XRD patterns of the S1–S4 samples.

In order to get more information about the appearance of the surfaces of the prepared samples, the SEM (Scanning Electron Microscopy) images were examined. The SEM electron microscopy images showing the morphology of the surfaces at different magnifications and the EDAX (Energy Dispersive X-ray) profiles are shown in Figure 2. Samples S1–S4 present porous structures with different surface morphologies, from small and uneven aggregates for S1–S3 to aggregates with an isometric structure for S4. The boundaries between the particles are not well defined.
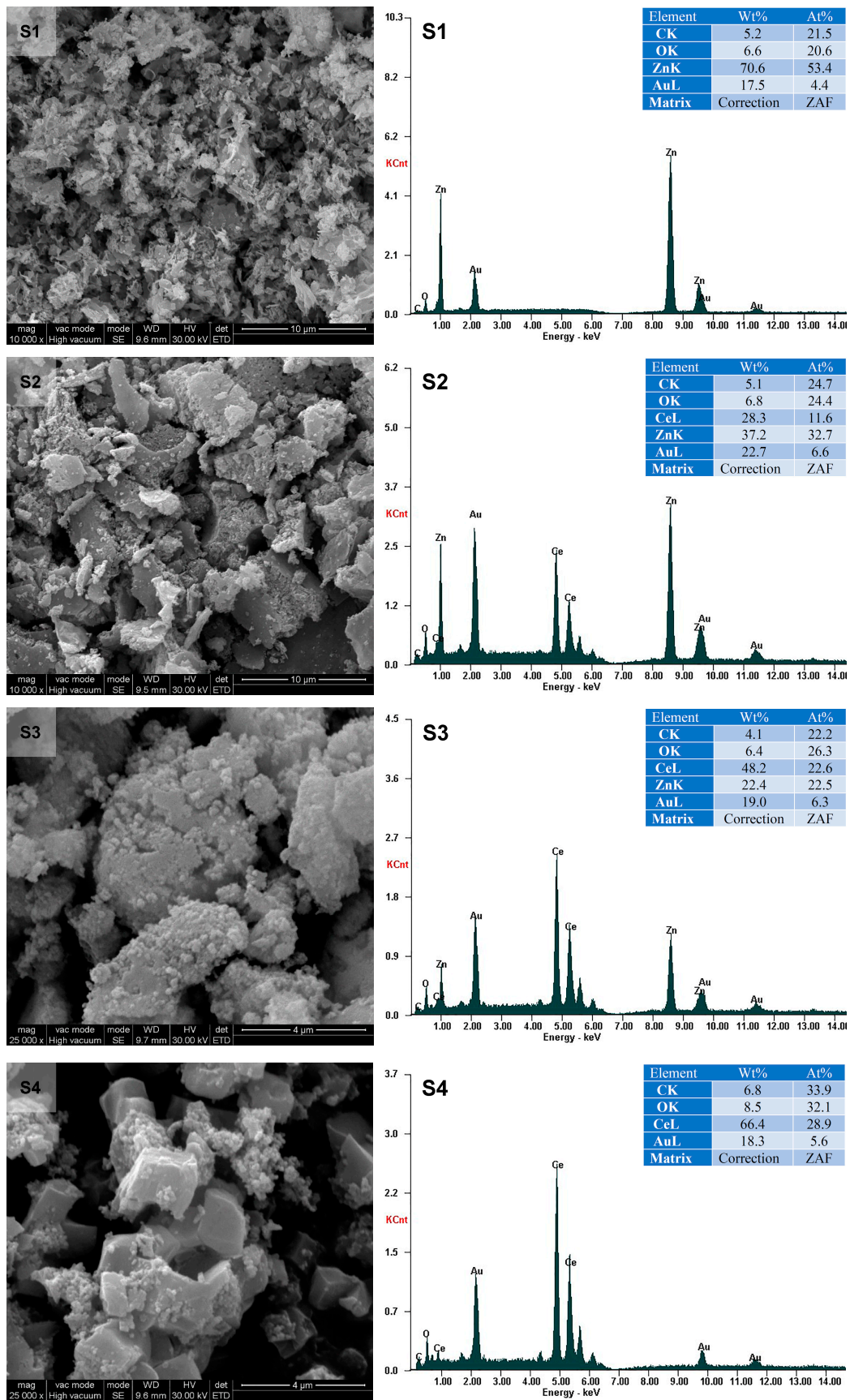
Figure 2. SEM micrographs (**left**) and EDAX pattern of the S1–S4 samples (**right**).

For S4, crystallite size varies from below 0.1 μm × 0.1 μm × 0.1 μm to approximately 1 μm × 2 μm × 3 μm. The accumulation of micro-crystallites is a normal process; the crystallites try to reach the minimum energy state, minimizing the contact area with the external environment. The small size of the obtained crystallites explains the good photocatalytic activity. EDAX analysis confirms the existence of Zn, Ce, and O elements, so CeO_2 and ZnO oxides are present.

The FTIR spectra are presented in Figure 3. FTIR analysis confirms that the organic phase has been eliminated by calcination. The peaks in the 3400–3450 cm^{-1} range are due to adsorbed water molecules (the O-H bond stretching vibration), and those in the 550–400 cm^{-1} range are generated by the vibrations of the metal oxide bonds [49,51].
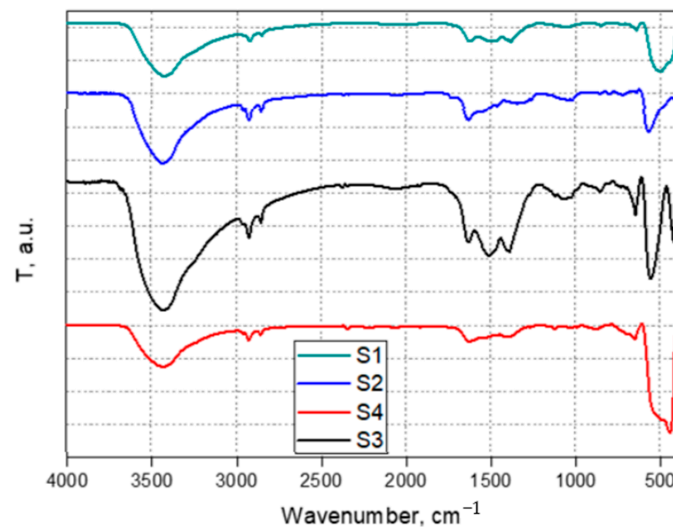

Figure 3. FTIR analysis of the synthesized samples.

Next, solid-state UV-Vis spectroscopy was used to obtain information on the optical properties of the synthesized samples and to calculate the E_g values (Figure 4). The optical band gap was determined using the Tauc formula, $(ah\nu)^2 = A(h\nu - E_g)$, in which a is the absorption coefficient, A is a constant, h is Planck's constant, ν is the frequency of incident radiation, E_g is the optical band gap, and n = 1/2 (for ZnO and CeO_2) [48,52]. The E_g values are obtained by extrapolating the straight lines to the point of intersection with the *x*-axis. Compared to pure ZnO and pure CeO_2, the composite materials S2 and S3 have a different E_g value.
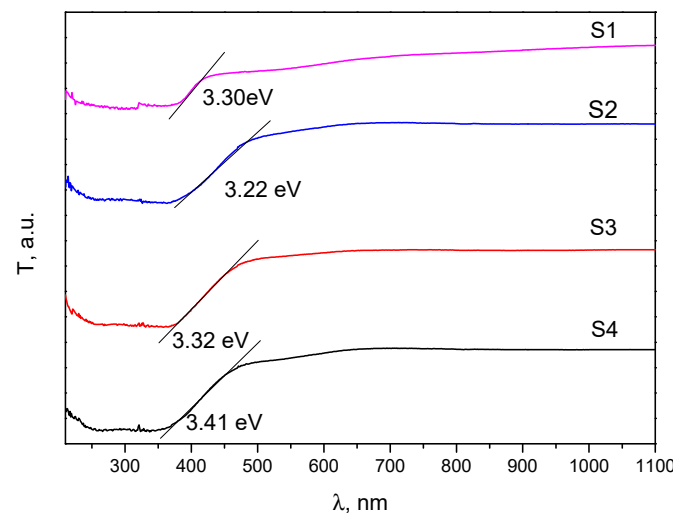

Figure 4. The optical absorption energy band gap estimated for CeO_2/ZnO samples.

The observed decrease in E_g values can be explained by the occurrence of numerous surface defect states such as oxygen vacancies, the coexistence of Ce^{4+} and Ce^{3+} in the CeO_2/ZnO heterostructure, and the interaction between ZnO and CeO_2 nanocrystals [53,54].
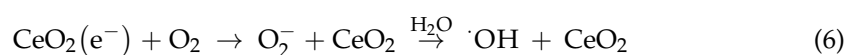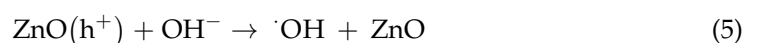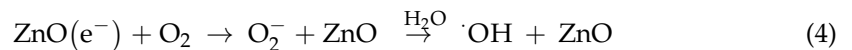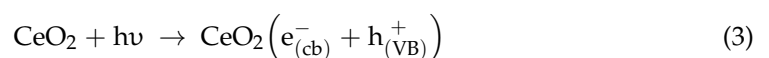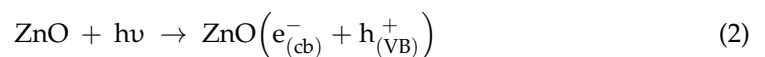
3.2. Antibiotic Photocatalytic Degradation

To evaluate the photocatalytic activity, the synthesized samples were contacted with solutions of chlortetracycline, ceftriaxone, and a chlortetracycline–ceftriaxone mixture (Figures 5–7). Work was carried out without adjustments to the natural pH value of the solutions. The doses of photocatalytic material have been studied previously; only the results for the 0.05 g·L^{-1} concentration are presented here. Experiments performed with UV irradiation but without a photocatalyst showed that both antibiotics are relatively stable to UV exposure. The experimental results have similar profiles; only a small fraction of the antibiotics is degraded after exposure to ultraviolet light in the absence of photocatalysts. The substantial increase in the photocatalytic performance of samples S2 and S3 compared to S1 and S4 (pure oxides) is due to the process of delaying the recombination of electron–hole pairs, owing to the formation of heterojunctions between the two oxides; this is advantageous for keeping the promoted electron in the conduction band of ZnO for a longer period of time. In this situation, adsorbed oxygen is more likely to form superoxide O_2^- radicals.
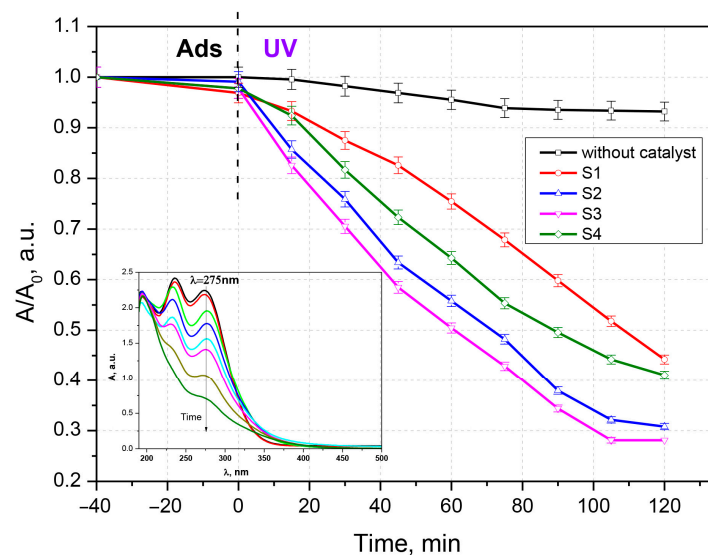
Figure 5. Photocatalytic degradation of chlortetracycline and time evolution of the UV-Vis absorption spectrum of chlortetracycline.

When CeO_2/ZnO —based photocatalytic materials are irradiated with UV rays, pairs of electric charge holes in the valence band and electric charge electrons in the conduction band are formed. The holes immediately react with water molecules or hydroxyl ions and form hydroxyl radicals, which are very strong oxidizing agents of organic molecules, according to the following Equations (2)–(9) [29,43,49]:

$$ZnO + h\upsilon \rightarrow ZnO\left(e_{(cb)}^- + h_{(VB)}^+\right) \tag{2}$$

$$CeO_2 + h\upsilon \rightarrow CeO_2\left(e_{(cb)}^- + h_{(VB)}^+\right) \tag{3}$$

$$ZnO\left(e^-\right) + O_2 \rightarrow O_2^- + ZnO \overset{H_2O}{\rightarrow} {}^\cdot OH + ZnO \tag{4}$$

$$ZnO\left(h^+\right) + OH^- \rightarrow {}^\cdot OH + ZnO \tag{5}$$

$$CeO_2\left(e^-\right) + O_2 \rightarrow O_2^- + CeO_2 \overset{H_2O}{\rightarrow} {}^\cdot OH + CeO_2 \tag{6}$$

$$CeO_2(h^+) + OH^- \rightarrow {}^{\cdot}OH + CeO_2 \tag{7}$$

$$Ce^{4+} + e^-_{(CB)} \rightarrow Ce^{3+} \tag{8}$$

$${}^{\cdot}OH + O_2^- + h^+_{(VB)} + \text{Antibiotic} \rightarrow \text{degradation products} \tag{9}$$
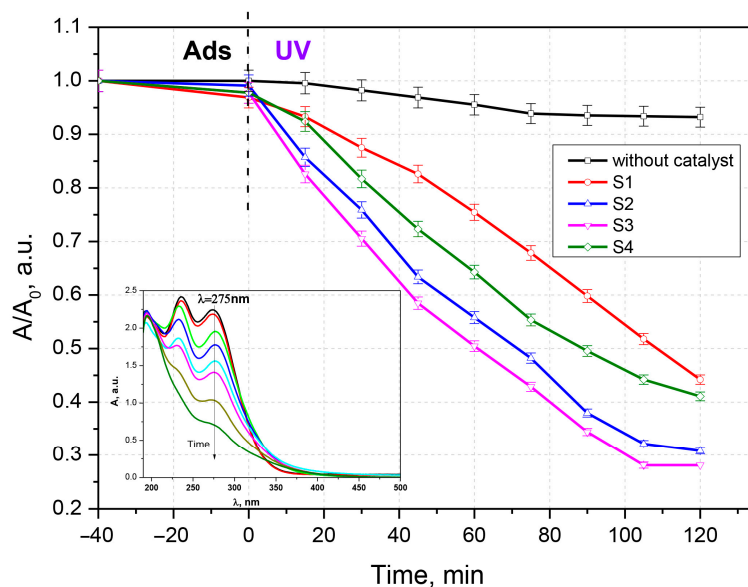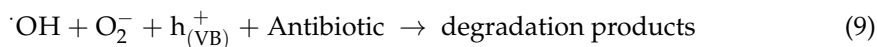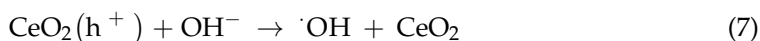

Figure 6. Photocatalytic degradation of ceftriaxone (**a**) and time evolution of the UV-Vis absorption spectrum of ceftriaxone.
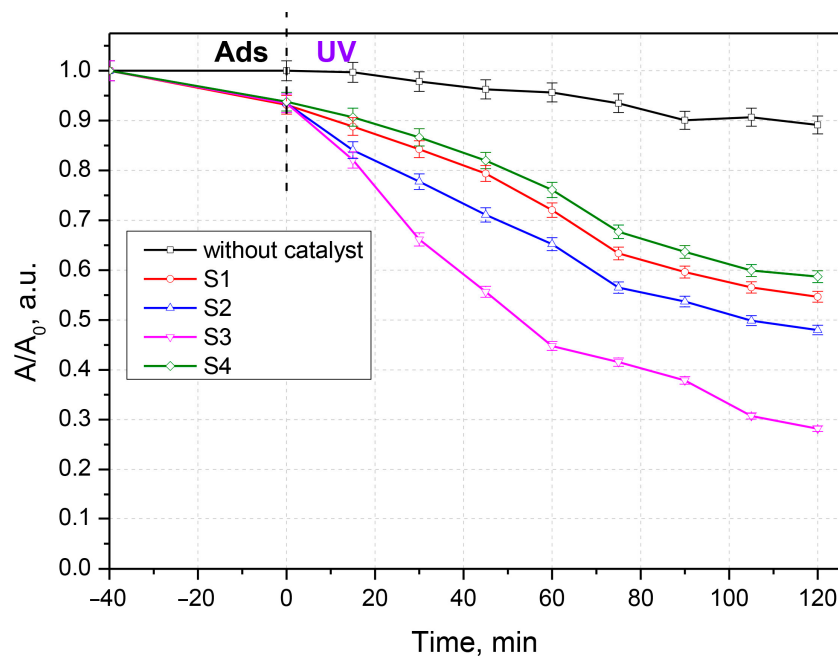
Figure 7. Photocatalytic degradation of the chlortetracycline + ceftriaxone mixture.

Oxidation processes of antibiotics take place in hole species (h^+) and O_2^-. Photocatalytic activity is influenced by crystal structure, specific surface area, particle size distribution, porosity, surface hydroxyl group density, etc. All these properties affect the formation of electron–hole pairs, the adsorption–desorption surface area, and the redox process. The photocatalytic activity of the studied materials was enhanced by delaying the recombination of electron–hole pairs. The main method of slowing down is through the

formation of heterojunctions in the CeO_2/ZnO mixture (Figure 8), a process described in other studies [49,52,53].
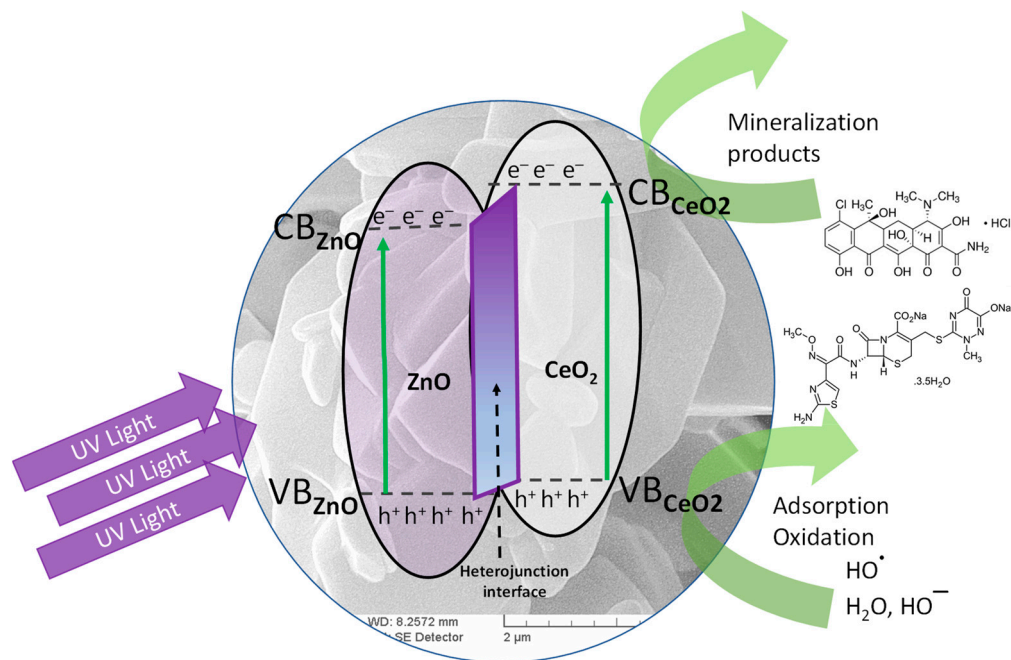
Figure 8. Proposed reaction mechanism for the photocatalytic activity of CeO_2/ZnO heterojunctions.

The electrons in the 4f orbitals of Ce interfere with the 3d electrons of Zn and the 2p electrons of O, resulting in the formation of a new band between BV and BC that changes the characteristics of the oxide mixture. The highest level of degradation was achieved for CFTX at 71.23% in the presence of S3, followed by CT at 58.65%, also for S3 (Figure 9). The higher proportion of CeO_2 in the synthesized materials has resulted in a higher degradation rate; Ce^{4+} ions act as a trap to prevent the recombination of electron–hole pairs generated by irradiation with ultraviolet rays, with $E > E_g$; thereby, the photocatalytic process is accelerated.
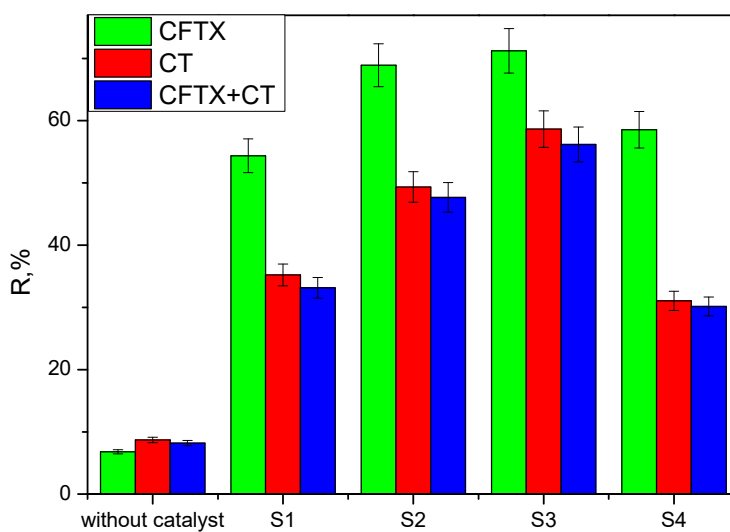
Figure 9. Degradation level for CFTX (ceftriaxone), CT (chlortetracycline) CFTX + CT (ceftriaxone+ chlortetracycline).

Compared to pure CeO_2 and pure ZnO, the superior catalytic performance of samples S2 and S3 is attributed to the formation of heterojunctions, which are an effective method for modifying the properties of mixed oxides.

The information gathered in Table 2 reveals the large diversity of materials that can be used as photocatalytic materials for ceftriaxone and tetracycline degradation.

Table 2. Summaries of the literature on the photodegradation of ceftriaxone and tetracycline.

Antibiotic (Target Pollutant)	Catalyst Type	Irradiation Source Power Intensity, Exposure Time, Mineralization Degree	Ref
Ceftriaxone	ZnO nanospherical particles supported TiO_2-nanorod MXene	Solar simulator 2000 550 W Max Lamp, 100 mW·cm^{-2}, 99.4%	[47]
Ceftriaxone C_0 = 16.5–66 μM	Bi_2WO_6 and g-C_3N_4 nanosheets	KrCl excilamp, 222 nm 23 W, incident irradiance—0.74 mW·cm^{-2}, 60 min	[55]
Ceftriaxone 20–100 mg·L^{-1}	Fenton-like oxidation process, persulphate activator, iron dosage—0.1–0.5 g·L^{-1} + scavengers (tert-butyl alcohol and isopropanol)	60 min, pH influence: 54.4% (pH: 5–6, Fe^{2+} dosage: 0.2 g·L^{-1}, PS concentration: 3 mM, initial antibiotic concentration: 20 mg·L^{-1}, UV power: 8 W: 20 °C) 95.7% (pH: 4.0, Fe^{2+} dosage: 0.3 g·L^{-1}, PS concentration: 4 Mm, UV, power: 8 W, 20 °C)	[27]
Ceftriaxone	Bi_2WO_6/g-C_3N_4	300 W Xe lamp, 120 min, 94.5%	[29]
Tetracycline, Oxytetracycline, Chlortetracycline	MoSSe nanohybrids	60 min 48.6% for TC 51.1% for OTC 56.5% for CTC	[56]
Oxytetracycline	MgAl calcined hydrotalcites	Pen Ray Power Supply 2.16 W MgAl-2.0, 59.32% for 5 h MgAl-2.5, 65.82% for 5 h MgAl-3, 63.87% for 5 h	[57]
Tetracycline	CeO_2-ZnO hetero photocatalyst	300 W Xenon lamp, 60 min, 87.25%	[53]
Tetracycline	$La_2Ti_2O_7$/AK—acid-modified coal-bearing strata kaolinite	300 W Xenon lamp $La_2Ti_2O_7$, 60 min, 57.11% $La_2Ti_2O_7$/CK, 60 min, 83.07% $La_2Ti_2O_7$/AK, 60 min, 88.61%	[58]

3.3. Kinetic Analysis

The photocatalytic process was assumed to follow a pseudo-first-order model according to Equation (10).

$$- k_{obs} \cdot t = \ln(C_t - C_0) = \ln(A_t - A_0) \tag{10}$$

where A_0 and A_t represent the absorbance of antibiotics solution measured at specific λ, initially and at t moment, and k_{obs} is the first-order oxidation rate constant (min^{-1}) [28,29,51]. The kinetic curves of the photocatalytic degradation of the two antibiotics with the prepared samples in 120 min are shown in Figures 10–12. According to this equation, if the experimental data show first-order kinetics, a line in the coordinates $-\ln(A/A_0)$ vs. t must be obtained. Therefore, a pseudo-first-order kinetic model was used to fit the experimental data presented in Figures 10–12. Fitting of the rate data using a higher reaction order does not generate good coefficients.

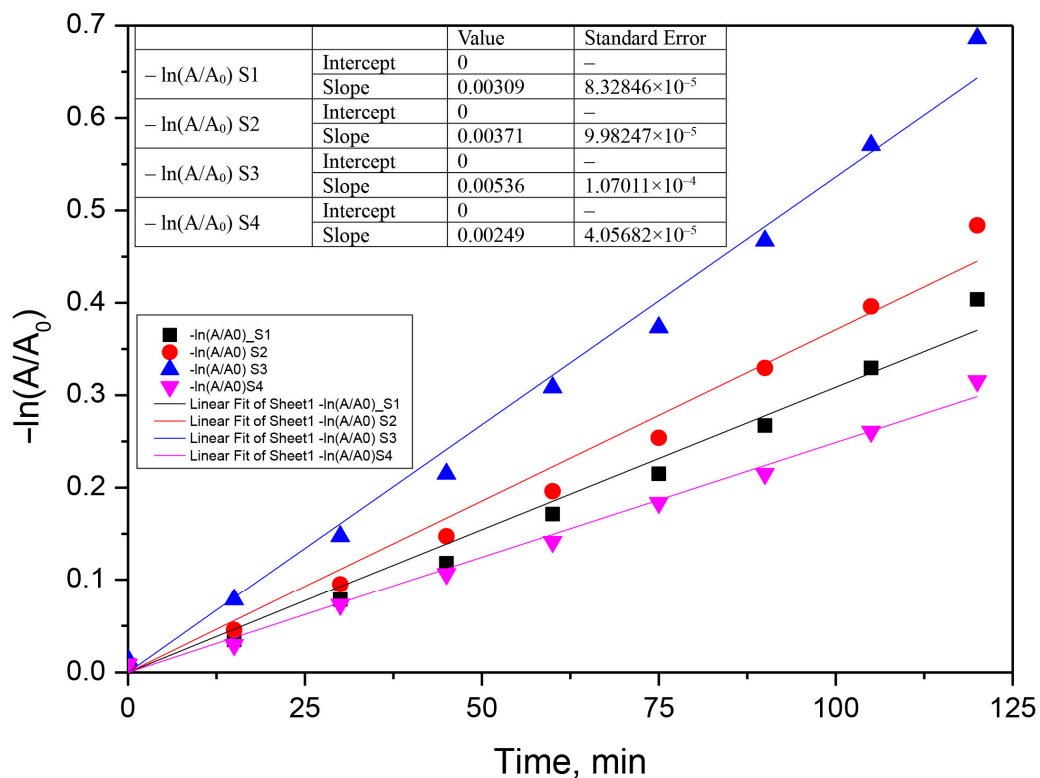**Figure 10.** Fits of the pseudo-first-order kinetic model for the photocatalytic chlortetracycline degradation using the S1–S4 photocatalyst (0.05 g·L^{-1}, chlortetracycline concentration 0.025 g·L^{-1}).
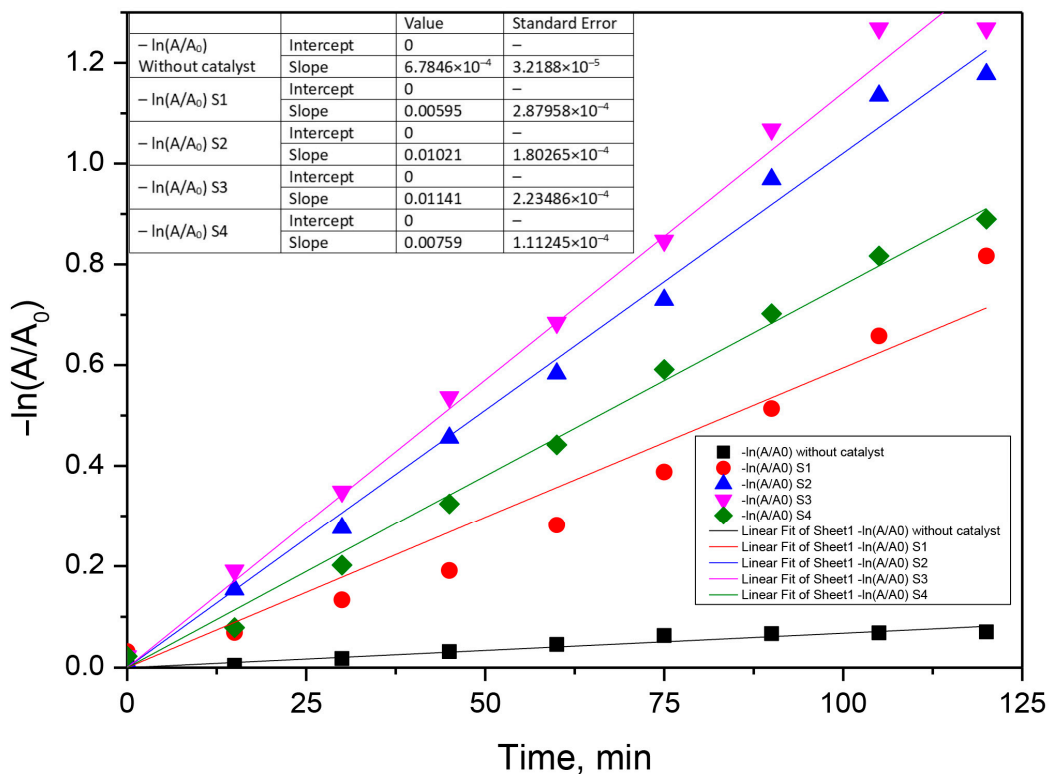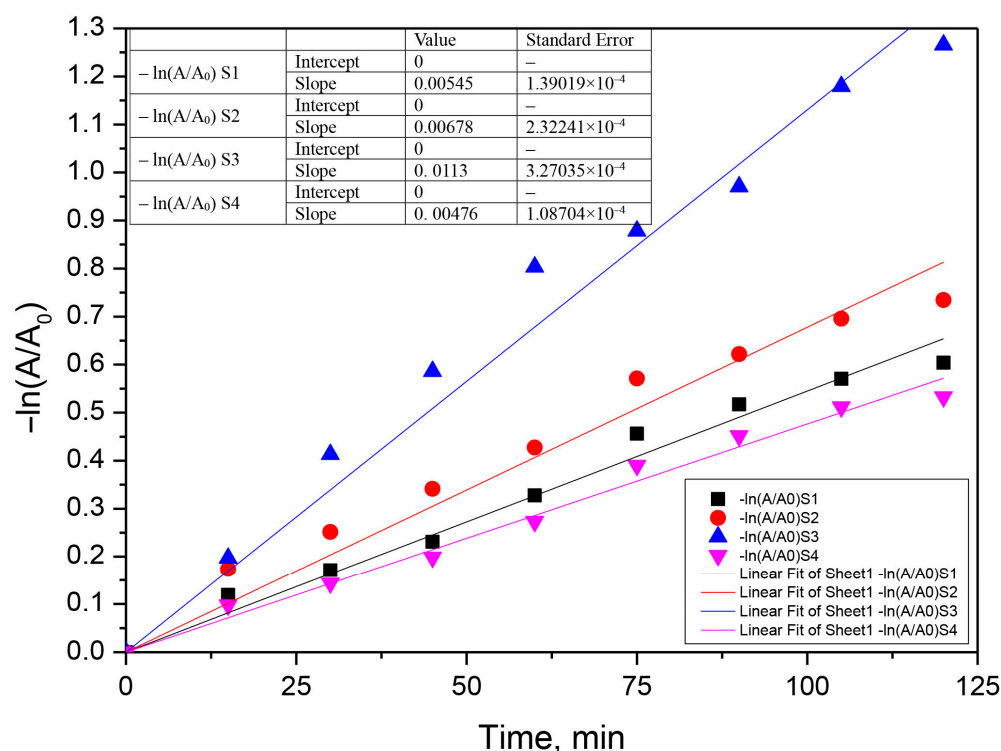

Figure 11. Fits of the pseudo-first-order kinetic model for the photocatalytic ceftriaxone degradation using the S1–S4 photocatalyst (0.05 g·L^{-1}, ceftriaxone concentration 0.05 g·L^{-1}).

		Value	Standard Error
$-\ln(A/A_0)$ S1	Intercept	0	–
	Slope	0.00545	1.39019×10^{-4}
$-\ln(A/A_0)$ S2	Intercept	0	–
	Slope	0.00678	2.32241×10^{-4}
$-\ln(A/A_0)$ S3	Intercept	0	–
	Slope	0.0113	3.27035×10^{-4}
$-\ln(A/A_0)$ S4	Intercept	0	–
	Slope	0.00476	1.08704×10^{-4}

Figure 12. Fits of the pseudo-first-order kinetic model for the photocatalytic chlortetracycline + ceftriaxone mixture degradation using the S1–S4 photocatalyst (0.05 g·L^{-1}, chlortetracycline concentration 0.025 g·L^{-1}, ceftriaxone concentration 0.05 g·L^{-1}).

4. Conclusions

In this work, we have reported a CeO$_2$/ZnO mixed oxide powder with good photocatalytic activity for the degradation of some antibiotics (ceftriaxone and chlortetracycline) that are relatively stable to UV radiation. Four samples were synthesized by the hydrothermal method, two of which were pure oxides (ZnO and CeO$_2$) and two of which were mixed oxides with different molar ratios (CeO$_2$/ZnO). These were characterized by XRD, FTIR, SEM + EDAX, and UV-Vis on the solid. All four samples showed photocatalytic activity to reduce the level of antibiotics in wastewater (CFTX, CT, and the mixture of the two); the experimental results showed that mixed oxides behave better than pure oxides (Ce:Zn ratio = 2.1) and have better photocatalytic activity in all three tested situations (CFTX, CT, CFTX + CT). Since the radiation dose used is very low and the synthesized materials are chemically inert, we consider that they are useful for reducing the level of antibiotics in wastewater. The heterogeneous photocatalytic processes have a net advantage in the reduction in some contaminants from the aqueous medium (antibiotics), including the non-selective breakdown of pollutants to very low concentrations, normal pressure and temperature, use of oxygen as the primary oxidant, and the possibility of simultaneously inducing both oxidation reactions and reduction reactions.

Author Contributions: Conceptualization, N.A., M.H. and G.A.A.; methodology, R.E.T.F., C.C. (Corina Cernatescu) and G.A.A.; validation, C.C. (Claudia Cobzaru) and M.A.V.; formal analysis, G.A.A. and R.E.T.F.; investigation, C.C. (Claudia Cobzaru) and C.C. (Corina Cernatescu); resources, M.H.; writing—original draft preparation, G.A.A., M.A.V. and N.A.; writing—review and editing, G.A.A. and M.H.; visualization, N.A.; supervision, M.H. and G.A.A. All authors have read and agreed to the published version of the manuscript.

Institutional Review Board Statement: Not applicable.

Informed Consent Statement: Not applicable.

Data Availability Statement: The data presented in this study are available on request from the corresponding authors.

Conflicts of Interest: The authors declare no conflict of interest.

References

1. World Health Organization. *World Health Organization Model List of Essential Medicines: 21st List 2019*; WHO/MVP/EMP/IAU/2019.06. License: CC BY-NC-SA 3.0 IGO. hdl:10665/325771; World Health Organization: Geneva, Switzerland, 2019. Available online: https://apps.who.int/iris/rest/bitstreams/1237479/retrieve (accessed on 10 May 2020).
2. Dan, A.; Zhang, X.; Dai, Y.; Chen, C.; Yang, Y. Occurrence and removal of quinolone, tetracycline, and macrolide antibiotics from urban wastewater in constructed wetlands. *J. Clean. Prod.* **2020**, *252*, 119677. [CrossRef]
3. Tetracycline Pharmacokinetics. Available online: https://www.drugs.com/monograph/tetracycline.html (accessed on 2 November 2022).
4. Rodriguez-Mozaz, S.; Vaz-Moreira, I.; Della Giustina, S.V.; Llorca, M.; Barceló, D.; Schubert, S.; Berendonk, T.U.; Michael-Kordatou, I.; Fatta-Kassinos, D.; Martinez, J.L.; et al. Antibiotic residues in final effluents of European wastewater treatment plants and their impact on the aquatic environment. *Environ. Int.* **2020**, *140*, 105733. [CrossRef] [PubMed]
5. Verma, T.; Aggarwal, A.; Singh, S.; Sharma, S.; Sarma, S.J. Current challenges and advancements towards discovery and resistance of antibiotics. *J. Mol. Struc.* **2022**, *1248*, 131380. [CrossRef]
6. Zahedi, S.; Gros, M.; Balcazar, J.L.; Petrovic, M.; Pijuan, M. Assessing the occurrence of pharmaceuticals and antibiotic resistance genes during the anaerobic treatment of slaughterhouse wastewater at different temperatures. *Sci. Total Environ.* **2021**, *789*, 147910. [CrossRef]
7. Zhang, Y.; Pei, M.; Zhang, B.; He, Y.; Zhong, Y. Changes of antibiotic resistance genes and bacterial communities in the advanced biological wastewater treatment system under low selective pressure of tetracycline. *Water Res.* **2021**, *207*, 117834. [CrossRef]
8. Li, J.; Zhang, K.; Zhang, H. Adsorption of antibiotics on microplastics. *Environ. Pollut.* **2018**, *237*, 460–467. [CrossRef]
9. Wang, K.; Zhuang, T.; Su, Z.; Chi, M.; Wang, H. Antibiotic residues in wastewaters from sewage treatment plants and pharmaceutical industries: Occurrence, removal and environmental. *Sci. Total Environ.* **2021**, *788*, 147811. [CrossRef]
10. Uluseker, C.; Kaster, K.M.; Thorsen, K.; Basiry, D.; Shobana, S.; Jain, M.; Kumar, G.; Kommedal, R.; Pala-Ozkok, I. A Review on Occurrence and Spread of Antibiotic Resistance in Wastewaters and in Wastewater Treatment Plants: Mechanisms and Perspectives. *Front. Microbiol.* **2021**, *12*, 717809. [CrossRef]
11. Shigei, M.; Assayed, A.; Hazaymeh, A.; Dalahmeh, S.S. Pharmaceutical and Antibiotic Pollutant Levels in Wastewater and the Waters of the Zarqa River, Jordan. *Appl. Sci.* **2021**, *11*, 8638. [CrossRef]
12. Imwene, K.O.; Ngumba, E.; Kairigo, P.K. Emerging technologies for enhanced removal of residual antibiotics from source-separated urine and wastewaters: A review. *J. Environ. Manag.* **2022**, *322*, 116065. [CrossRef]
13. Nasrollahi, N.; Vatanpour, V.; Khataee, A. Removal of antibiotics from wastewaters by membrane technology: Limitations, successes, and future improvements. *Sci. Total Environ.* **2022**, *838 (Pt 1)*, 156010. [CrossRef]
14. Masood, Z.; Ikhlaq, A.; Farooq, A.; Qi, F.; Javed, F.; Aziz, H.A. Removal of anti-biotics from veterinary pharmaceutical wastewater using combined Electroflocculation and Fe-Zn loaded zeolite 5A based catalytic ozonation process. *J. Water Process. Eng.* **2022**, *49*, 103039. [CrossRef]
15. Phoon, B.L.; Ong, C.C.; Shuai, M.; Saheed, M.; Show, P.L.; Chang, J.S.; Ling, T.C.; Lam, S.S.; Juan, J.C. Conventional and emerging technologies for removal of antibiotics from wastewater. *J. Hazard Mater.* **2020**, *400*, 122961. [CrossRef] [PubMed]
16. Foroughi, M.; Khiadani, M.; Kakhki, S.; Kholghi, V.; Naderi, K.; Yektay, S. Effect of ozonation-based disinfection methods on the removal of antibiotic resistant bacteria and resistance genes (ARB/ARGs) in water and wastewater treatment: A systematic review. *Sci. Total Environ.* **2022**, *811*, 151404. [CrossRef] [PubMed]
17. Chu, L.; Wang, J.; He, S.; Chenc, C.; Wojnárovits, L.; Takács, E. Treatment of pharmaceutical wastewater by ionizing radiation: Removal of antibiotics, antimicrobial resistance genes and antimicrobial activity. *J. Hazard Mater.* **2021**, *415*, 125724. [CrossRef]
18. Lan, L.; Kong, X.; Sun, X.; Li, C.; Liu, D. High removal efficiency of antibiotic resistance genes in swine wastewater via nanofiltration and reverse osmosis processes. *J. Environ. Manag.* **2019**, *231*, 439–445. [CrossRef]
19. Leng, L.; Wei, L.; Xiong, Q.; Xu, S.; Li, W.; Lv, S.; Lu, Q.; Wan, L.; Wen, Z.; Zhou, W. Use of microalgae based technology for the removal of antibiotics from wastewater: A review. *Chemosphere* **2020**, *238*, 124680. [CrossRef]
20. Guo, Z.; Huo, W.; Cao, T.; Liu, X.; Ren, S.; Yang, J.; Ding, H.; Chen, K.; Dong, F.; Zhang, Y. Heterojunction interface of zinc oxide and zinc sulfide promoting reactive molecules activation and carrier separation toward efficient photocatalysis. *J. Colloid Interface Sci.* **2021**, *588*, 826–837. [CrossRef]
21. Harja, M.; Ciobanu, G. Studies on adsorption of oxytetracycline from aqueous solutions onto hydroxyapatite. *Sci. Total Environ.* **2018**, *628–629*, 36–43. [CrossRef]
22. Sanguanpak, S.; Shongkittikul, W.; Saengam, C.; Chiemchaisri, W.; Chiemchaisri, C. TiO2-immobilized porous geopolymer composite membrane for removal of antibiotics in hospital wastewater. *Chemosphere* **2022**, *307 (Pt 2)*, 135760. [CrossRef]
23. Wang, Y.; Sun, T.; Tong, L.; Gao, Y.; Zhang, H.; Zhang, Y.; Wang, Z.; Zhu, S. Non-free Fe dominated PMS activation for enhancing electro-Fenton efficiency in neutral wastewater. *J. Electroanal. Chem.* **2023**, *928*, 117062. [CrossRef]

24. Huang, Z.; Cao, S.; Yu, J.; Tang, X.; Guo, Y.; Guo, Y.; Wang, L.; Dai, S.; Zhan, W. Total Oxidation of Light Alkane over Phosphate-Modified Pt/CeO$_2$ Catalysts. *Environ. Sci. Technol.* **2022**, *56*, 9661–9671. [CrossRef] [PubMed]

25. Rodríguez-Chueca, J.; della Giustina, S.V.; Rocha, J.; Fernandes, T.; Pablos, C.; Encinas, A.; Barceló, D.; Rodríguez-Mozaz, S.; Manaia, C.M.; Marugán, J. Assessment of full-scale tertiary wastewater treatment by UV-C based-AOPs: Removal or persistence of antibiotics and antibiotic resistance genes? *Sci. Total Environ.* **2019**, *652*, 1051–1061. [CrossRef] [PubMed]

26. Sacco, O.; Vaiano, V.; Rizzo, L.; Sannino, D. Intensification of ceftriaxone degradation under UV and solar light irradiation in presence of phosphors based structured catalyst. *Chem. Eng. Process.* **2019**, *137*, 12–21. [CrossRef]

27. Kordestani, B.; Yengejeh, R.J.; Takdastan, A.; Neisi, A.K. A new study on photocatalytic degradation of meropenem and ceftriaxone antibiotics based on sulfate radicals: Influential factors, biodegradability, mineralization approach. *Microchem. J.* **2019**, *146*, 286–292. [CrossRef]

28. Abramović, B.F.; Uzelac, M.M.; Armaković, S.J.; Gašić, U.; Četojević-Simin, D.D.; Armaković, S. Experimental and computational study of hydrolysis and photolysis of antibiotic ceftriaxone: Degradation kinetics, pathways, and toxicity. *Sci. Total Environ.* **2021**, *768*, 144991. [CrossRef] [PubMed]

29. Zhao, Y.; Liang, X.; Wang, Y.; Shi, H.; Liu, E.; Fan, J.; Hu, X. Degradation and removal of Ceftriaxone sodium in aquatic environment with Bi$_2$WO$_6$/g-C$_3$N$_4$ photocatalyst. *J. Colloid Interface Sci.* **2018**, *523*, 7–17. [CrossRef]

30. Kurt, A.; Mert, B.K.; Özengin, N.; Sivrioğlu, Ö.; Yonar, T. Treatment of Antibiotics in Wastewater Using Advanced Oxidation Processes (AOPs). In *Physico-Chemical Wastewater Treatment and Resource Recovery*; Farooq, R., Ahmad, Z., Eds.; IntechOpen: London, UK, 2017. [CrossRef]

31. Lwin, H.M.; Zhan, W.; Song, S.; Jia, F.; Zhou, J. Visible-light photocatalytic degradation pathway of tetracycline hydrochloride with cubic structured ZnO/SnO$_2$ heterojunction nanocatalyst. *Chem. Phys. Lett.* **2019**, *736*, 136806. [CrossRef]

32. de Moraes, N.P.; de Campos Sanmartin, M.B.; da Silva Rocha, R.; de Siervo, A.; de Vasconcelos Lanza, M.R.; Reddy, D.A.; Lianqing, Y.; Alvares Rodrigues, L. ZnO/CeO$_2$/Carbon xerogel composites with direct Z-scheme heterojunctions: Enhancing the photocatalytic remediation of 4-chlorophenol under visible light. *J. Rare Earths* **2022**, *in press*. [CrossRef]

33. Kashmery, H.A.; El-Hout, S.I.; Zak, Z.I. Fast photocatalytic oxidation of ciprofloxacin over Co$_3$O$_4$@CeO$_2$ heterojunctions under visible-light. *J. Taiwan Inst. Chem. Eng.* **2022**, *140*, 104563. [CrossRef]

34. Montini, T.; Melchionna, M.; Monai, M.; Fornasiero, P. Fundamentals and Catalytic Applications of CeO$_2$-Based Materials. *Chem. Rev.* **2016**, *116*, 5987–6041. [CrossRef] [PubMed]

35. Fauzi, A.A.; Jalila, A.A.; Hassan, N.S.; Aziz, F.F.A.; Azami, M.S.; Hussain, I.; Saravanan, R.; Vo, D.-V.N. A critical review on relationship of CeO$_2$-based photocatalyst towards mechanistic degradation of organic pollutant. *Chemosphere* **2022**, *286*, 131651. [CrossRef] [PubMed]

36. Latif, M.M.; Haq, A.U.; Amin, F.; Ajaz-un-Nabi, M.; Khan, I.; Sabir, N. Synthesis and antimicrobial activities of Manganese (Mn) and iron (Fe) co-doped Cerium dioxide (CeO$_2$) Nanoparticles. *Physica B Condens. Matter.* **2021**, *600*, 412562. [CrossRef]

37. Rajeshkumar, S.; Naik, P. Synthesis and biomedical applications of Cerium oxide nanoparticles—A Review. *Biotechnol. Rep.* **2018**, *17*, 1–5. [CrossRef] [PubMed]

38. Parvathy, S.; Subramanian, P.; Karthick, S.A.; Subbaiya, R. The structural, optical, antimicrobial and anticancer properties of biocompatible astaxanthin coated ZnO and CeO$_2$ nanoparticles. *Mater. Lett.* **2022**, *312*, 131669. [CrossRef]

39. Gao, W.; Liu, Y.; Dong, J. Immobilized ZnO based nanostructures and their environmental applications. *Prog. Nat. Sci. Mater Int.* **2021**, *31*, 821–834. [CrossRef]

40. Noman, M.T.; Amor, N.; Petru, M. Synthesis and applications of ZnO nanostructures (ZONSs): A review. *Crit. Rev. Solid State Mater. Sci.* **2022**, *47*, 99–141. [CrossRef]

41. Sescu, A.M.; Harja, M.; Favier, L.; Berthou, L.O.; Gomez de Castro, C.; Pui, A.; Lutic, D. Zn/La mixed oxides prepared by coprecipitation: Synthesis, characterization and photocatalytic studies. *Materials* **2020**, *13*, 4916. [CrossRef]

42. Khankhuean, A.; Kuratsameethong, W.; Santibenchakul, S.; Laobuthee, A.; Sugimoto, M.; Srisawat, N.; Jamnongkan, T. Oriented ZnO nanoflowers obtained after calcination of electrospinning poly(vinyl alcohol)/zinc oxide/zinc acetate composite mats. *S. Afr. J. Chem. Eng.* **2021**, *37*, 179–185. [CrossRef]

43. Apostolescu, N.; Cernătescu, C.; Tătaru-Fărmuș, R.E.; Cobzaru, C.; Apostolescu, G.A. Promoting Effect of Ceria on the Catalytic Activity of CeO$_2$-ZnO Polycrystalline Materials. *Environ. Eng. Manag. J.* **2018**, *17*, 765–770.

44. Vojtová, V.; Urbánek, K. Pharmacokinetics of tetracyclines and glycylcyclines. *Klin. Mikrobiol. Infekc. Lek.* **2009**, *15*, 17–21. [PubMed]

45. SigmaAldrich. Available online: https://www.sigmaaldrich.com/RO/en/sds/sigma/c4881 (accessed on 11 December 2021).

46. Patel, I.H.; Kaplan, S.A. Pharmacokinetic profile of ceftriaxone in man. *Am. J. Med.* **1984**, *77*, 17–25. [PubMed]

47. Abbas, K.K.; AbdulkadhimAl-Ghaban, A.M.H.; Rdewi, E.H. Synthesis of a novel ZnO/TiO$_2$-nanorod MXene heterostructured nanophotocatalyst for the removal pharmaceutical ceftriaxone sodium from aqueous solution under simulated sunlight. *J. Environ. Chem. Eng.* **2022**, *10*, 108111. [CrossRef]

48. Li, S.; Zhang, Y.; Han, L.; Li, X.; Xu, Y. Highly sensitive and selective triethylamine gas sensor based on hierarchical radial CeO$_2$/ZnO n-n heterojunction. *Sens. Actuators B Chem.* **2022**, *367*, 132031. [CrossRef]

49. Meenakshi, G.; Sivasamy, A. Enhanced photocatalytic activities of CeO$_2$@ZnO core-shell nanostar particles through delayed electron hole recombination process. *Colloids Surf. A Physicochem. Eng. Asp.* **2022**, *645*, 128920. [CrossRef]

50. Rosi, H.; Janci, M.; Preethi, M. Phyto-mediated green synthesis of CeO_2–ZnO nanoparticles using glycosmis mauritiana leaf extract: Antibacterial activity and photodegradative applications. *Mater. Today Proc.* **2022**, *48*, 561–567. [CrossRef]

51. Duarte, F.d.S.; Melo, A.L.M.d.S.; Ferro, A.d.B.; Zanta, C.L.d.P.e.S.; Duarte, J.L.d.S.; Oliveira, R.M.P.B. Magnetic Zinc Oxide/Manganese Ferrite Composite for Photodegradation of the Antibiotic Rifampicin. *Materials* **2022**, *15*, 8185. [CrossRef]

52. Ma, L.; Ai, X.; Jiang, W.; Liu, P.; Chen, Y.; Lu, K.; Song, X.; Wu, X. Zn/Ce metal organic framework-derived ZnO@CeO_2 nano-heterojunction for enhanced photocatalytic activity. *Colloid Interface Sci. Commun.* **2022**, *49*, 100636. [CrossRef]

53. Ye, Z.; Li, J.; Zhou, M.; Wang, H.; Ma, Y.; Huo, P.; Yu, L.; Yan, Y. Well-dispersed nebula-like ZnO/CeO_2@HNTs heterostructure for efficient photocatalytic degradation of tetracycline. *Chem. Eng. J.* **2016**, *304*, 917–933. [CrossRef]

54. Al-Bataineh, Q.M.; Telfah, M.; Ahmad, A.A.; Alsaad, A.M.; Qattan, I.A.; Baaziz, H.; Charifi, Z.; Telfah, A. Synthesis, Crystallography, Microstructure, Crystal Defects, Optical and Optoelectronic Properties of ZnO:CeO_2 Mixed Oxide Thin Films. *Photonics* **2020**, *7*, 112. [CrossRef]

55. Sizykh, M.; Batoeva, M.; Matafonova, G. Enhanced catalyst-free degradation and mineralization of ceftriaxone by UV/H_2O_2 and UV/$S_2O_8{}^{2-}$ processes using KrCl excilamp (222 nm). *J. Photochem. Photobiol. A Chem.* **2023**, *436*, 114357. [CrossRef]

56. Chen, L.; Chen, C.-W.; Huang, C.P.; Chuang, Y.; Nguyen, T.B.; Dong, C.D. A visible-light sensitive MoSSe nanohybrid for the photocatalytic degradation of tetracycline, oxytetracycline, and chlortetracycline. *J. Colloid Interface Sci.* **2022**, *616*, 67–80. [CrossRef] [PubMed]

57. Jácome-Acatitla, G.; Tzompantzi, F.; López-González, R.; García-Mendoza, C.; Alvaro, J.M.; Gomez, R. Photodegradation of sodium naproxen and oxytetracycline hydrochloride in aqueous medium using as photocatalysts Mg-Al calcined hydrotalcites. *J. Photochem. Photobiol. A Chem.* **2014**, *277*, 82–89. [CrossRef]

58. Zhao, Y.; Cao, Z.; Li, J.; Bai, B.; Jia, Y.; Wang, Q.; Cheng, H. Selective adsorption and photocatalytic degradation of chlortetracycline hydrochloride using a $La_2Ti_2O_7$/acid-modified coal-bearing strata kaolinite composite. *Appl. Surf. Sci.* **2023**, *609*, 155489. [CrossRef]